Diffraction Signals of Aligned Molecules in the Gas Phase: Tetrazine in Intense Laser Fields

Seol Ryu, Richard M. Stratt, and Peter M. Weber*

Department of Chemistry, Brown University, Providence, Rhode Island 02912

Received: April 17, 2003; In Final Form: June 30, 2003

We performed a theoretical study of the electron diffraction patterns that arise from aligning a molecule, *s*-tetrazine ($C_2N_4H_2$), in a high intensity laser field using the Friedrich−Herschbach approach. The molecule is modeled using geometries and zero-point vibrations from a coupled-cluster level ab initio calculation. The alignment is achieved by a circularly polarized, quasicontinuous high-intensity laser pulse that intersects the molecular sample at selected geometries. The molecular ensemble is taken to be at a rotational temperature of 5 K. We find that even at 1 TW/cm^2 there is a very noticeable effect on the diffraction pattern stemming from the alignment. Moreover, using different laser geometries, it is possible to observe different diffraction patterns corresponding to specific projections of the molecular geometry onto the Fourier plane of the detector, making the laser a kind of "optical goniometer." Predictably, higher alignment laser intensities lead to narrower orientational distributions, which in turn provide for diffraction patterns with larger modulation depths. We find, however, that for small diffraction angles ($s \leq 15$ Å^{-1}) the effect appears to saturate at an alignment laser intensity of about 4 TW/cm^2. This suggests that there is a window of opportunity where alignment is very beneficial for extracting information from gas-phase diffraction patterns and where detrimental multiphoton processes do not yet compromise the interpretation of the molecular structure.

I. Introduction

Conventional gas-phase electron diffraction patterns are often modeled using the expression

$$I_{\text{total}}(s) = I_{\text{atomic}}(s) + I_{\text{mol}}(s) \quad (1)$$

where $I_{\text{total}}(s)$ is the total scattering intensity as a function of the absolute value of the scattering vector, $\boldsymbol{s}$, and $I_{\text{atomic}}(s)$ and $I_{\text{mol}}(s)$ are the contributions from atomic and molecular scattering, respectively.[1] The atomic scattering, which is the given by the Rutherford scattering cross section and the atomic form factors,[2] is featureless and contains no information about the molecular structure. The molecular scattering signal contains the terms arising from all pairs of scattering centers and therefore contains the desired information about the molecular structure and the vibrational amplitudes. Unfortunately, in samples consisting of isotropic mixtures of gas phase molecules, the molecular term is significantly smaller than the atomic term, amounting to only a few percent of the total scattering in molecules without much symmetry.

The expression of eq 1 is somewhat deceptive, in that it may be construed to imply literally that the diffraction pattern is indeed composed of distinct and additive atomic and molecular *intensities*. Such an interpretation would, of course, be incorrect. Diffraction is an interference phenomenon, and the observed intensity arises from the interference of the scattered wavelets from all scattering centers. As such, it has the potential to be fully modulated. The reason for the small modulation depth observed in gas phase electron diffraction is therefore to be found in the isotropic nature of the gas phase sample. Indeed, the diffraction patterns of perfectly clamped molecular systems are fully modulated. This can be seen by examining the fundamental diffraction formulas or by inspection of the specific calculations for diatomic[3] and triatomic systems.[4] Moreover, the diffraction patterns of molecular crystals can be understood as the superposition of the fully modulated pattern from the clamped molecule and the Bragg scattering off the planes of the crystal lattice.[5] It therefore stands to reason that, if it were possible to align a gas-phase sample of molecules, some of the washed-out modulation depth of the total scattering signal might be recovered. The present paper investigates this signal recovery on the example of the 8-atomic molecule *s*-tetrazine, $C_2N_4H_2$.

Traditional approaches to align molecules have been based on electric multipole fields.[6,7] More recently, the increasing availability of very high-intensity laser pulses has stimulated the development of schemes that use quasicontinuous intense electromagnetic fields[8] or cleverly timed pulsed fields.[9] For our model studies, we chose the quasicontinuous alignment scheme considered by Zon and Katsnel'son,[10] and developed by Friedrich and Herschbach.[8] In this scheme, the AC electric field of the intense laser interacts with the polarizable electrons of the target molecule. Any anisotropy in the polarizability tensor of the molecule leads to a preferential alignment of the molecule such that the axis of the largest polarizability aligns with the laser field. To achieve the necessary laser fields, experiments typically take advantage of pulsed laser systems. However, for our simulations, we assume that the pump−probe diffraction experiment is on a time-scale much shorter than the alignment laser pulse, so that the alignment laser pulse can be assumed to be continuous. Because typical alignment laser pulses have durations on the order of 100 ps to several nanoseconds, this implies that our experiment is performed on a time-scale of not more than several picoseconds. Electron diffraction experiments on that time scale are quite feasible.[11] Indeed, early results by

* To whom correspondence should be addressed.

10.1021/jp0304632 CCC: $25.00
Published on Web 08/05/2003

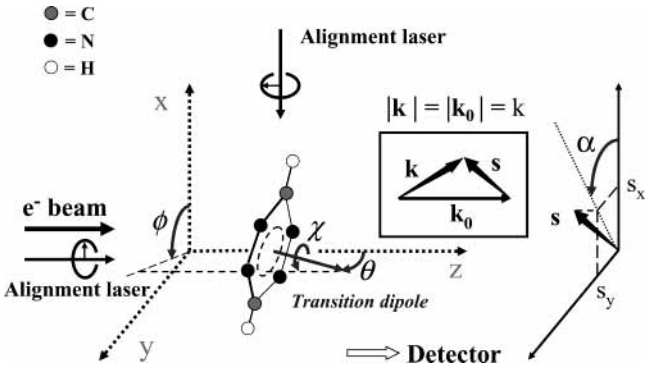

Figure 1. Coordinate system used to discuss electron diffraction from aligned s-tetrazine molecules. The three Euler angles (θ, ϕ, χ) are defined as the orientation of the transition dipole moment of the molecule with respect to the laboratory axes. The inset shows the momentum transfer vector $\mathbf{s} = \mathbf{k} - \mathbf{k}_0$, where $\mathbf{k}_0$ and $\mathbf{k}$ are the initial and final wave vectors of the electron, respectively. Circularly polarized lasers, aligned either collinearly or perpendicularly to the electron beam, induce the molecular alignment.

Hoshina et al. on the diffraction of electrons off high-intensity laser aligned molecules already show some of the expected effects.[12]

In the present paper, we seek to explore just how much the modulation depth of gas-phase diffraction patterns be can improved by the alignment of molecules in high-intensity laser fields. As we will see, using laser fields that are well within the reach of experimentalists to date, we should expect to observe a very significant effect on the diffraction patterns. The effect is most pronounced at small scattering angles, but it does extend to the largest scattering angles we have investigated (s up to 50 Å^{-1}). Moreover, because the alignment of the molecular ensemble depends on the polarization of the alignment laser, it is possible to turn the molecule so that different faces point toward the electron beam. In this way, one can "look" at the molecule from different sides, offering a significant enhancement of the information content of the diffraction patterns, as compared to the patterns from isotropic samples. Although the partial alignment obtained in weak alignment laser fields may make the analysis of the diffraction patterns difficult, we find that, depending on the orientation, the molecules can be aligned so well that their diffraction patterns hardly differ from those of perfectly clamped molecules. This apparent convergence to the fully clamped patterns can greatly aid the interpretation of diffraction patterns of aligned molecules.

II. Theoretical Methods

A. Molecular Alignment. In the alignment scheme proposed by Friedrich and Herschbach,[8] the direction of the laser beam defines a preferred orientation axis for the molecule. Opposing this alignment is the motion of the molecules in thermally populated rotational states. For this reason, the scheme requires environments with very low rotational temperatures, such as found in free jet expansions. Several reports have been published that demonstrate the feasibility of the Friedrich/Herschbach alignment scheme.[13]

Referring to Figure 1, we define the orientation of the tetrazine molecules by the three Euler angles θ, ϕ, and χ. The first two angles describe the orientation of the vector normal to the plane of the molecule with respect to the laboratory-frame Cartesian coordinates x, y, and z. The angle χ refers to the rotation of the molecule in the molecular plane. It is defined by the orientation of the long axis of the molecule, which cuts through the carbon and hydrogen atoms, with respect to the x axis.

The electron beam is assumed to enter from the negative z coordinate, and the diffraction image is projected in the x,y plane at large positive z values. The result of the scattering process is characterized by the vector **s**, which is the difference between the wave vector of the diffracted electron, **k**, and that of the incoming electron, $\mathbf{k}_0$. In our results, we report the projection of the scattering vector onto the x,y plane of the detector, $s_{proj} = (s_x^2 + s_y^2)^{1/2}$, a quantity that approaches the magnitude of the total scattering vector for small diffraction angles. The diffraction pattern is further characterized by its dependence on the angle $\alpha = \tan^{-1}(s_y/s_x)$, which is measured from the x axis.

The molecular property that determines the response of the molecule to the alignment laser is the polarizability tensor. For the three components of static polarizability of tetrazine in its ground-state electronic state, we used the values obtained from a CASPT2 calculation by Schütz et al.[14,15] They are 60.0 and 55.1 au for the in-plane directions and 32.6 a.u for the out-of-plane direction. Because the polarizability components for the in-plane direction are very similar, one should not expect to observe a significant alignment of the molecule regarding the rotation along the χ coordinate. To simplify the discussion, we therefore chose to use a circularly polarized alignment laser. In this scheme, the molecules are therefore free to rotate about the χ angle, and the alignment is only referring to the orientation of the plane of the molecule. We point out, however, that Larsen et al. have achieved a full alignment of a different molecule in all directions using an elliptically polarized alignment laser.[16]

For a molecule whose electronic transitions frequencies are well removed from that of the aligning laser, it has been shown in the literature[8,10,17] that it is possible to write an effective, time-independent Hamiltonian governing the molecule's orientation

$$\bar{H}_{\mathrm{ind}} = -\frac{1}{4}\vec{E}\cdot\bar{\bar{\alpha}}\cdot\vec{E} \tag{2}$$

where $\bar{\bar{\alpha}}$ is the molecular static polarizability tensor (whose components depend on the molecular orientation whenever the polarizability is anisotropic) and $\vec{E}$ is the static electric field vector describing the aligning pulses. In the examples we study in this paper, we are largely interested in using light fields circularly polarized in the laboratory xy plane, for which

$$\bar{H}_{\mathrm{ind}} = -\frac{1}{8}E_0^2(\alpha_{xx} + \alpha_{yy}) \tag{3}$$

with E_0 the magnitude of the field and α_{xx} and α_{yy} the components of the polarizability tensor in the laboratory frame, although we will also make use of the equivalent expression for the aligning laser circularly polarized in the laboratory yz plane

$$\bar{H}_{\mathrm{ind}} = -\frac{1}{8}E_0^2(\alpha_{yy} + \alpha_{zz}) \tag{4}$$

To determine the effect of the field on the molecular orientation, the effective Hamiltonian is expressed in the symmetric top basis representation $|JKM\rangle$[18] and diagonalized to find its eigenvalues and eigenfunctions. The evaluation of the matrix elements $\langle J'K'M'|\bar{H}_{\mathrm{ind}}|JKM\rangle$ involves the Wigner rotation matrix elements $\langle J'K'M'|D^1_{q's'}D^1_{qs}|JKM\rangle$, which can be calculated by expanding as $\sum_{jkm}\langle J'K'M'|D^1_{q's'}|jkm\rangle\langle jkm|D^1_{qs}|JKM\rangle$.[9] Alternatively, we can

directly calculate the matrix elements by substituting explicit expressions for $|JKM\rangle$ and $\bar{H}_{\text{ind}}$ as shown in the Appendix.

After collecting the eigenenergies $\{E_i\}$ and the eigenfunctions $\{\psi_i\}$, we find that the thermally averaged orientation probability density $\rho(\Omega)$ with Ω denoting the three Euler angles θ, ϕ, and χ is given by

$$\rho(\Omega) = \sum_i |\psi_i|^2 e^{-E_i/k_B T} \Big/ \sum_i e^{-E_i/k_B T} \tag{5}$$

with the distribution normalized so that

$$\int_0^{2\pi}\int_0^{2\pi}\int_0^{\pi} \rho(\theta,\phi,\chi) \sin\theta \, d\theta \, d\phi \, d\chi = 1$$

In our simulation, we used 1771 symmetric top basis functions with a maximum J value of 10. This provides a distribution function that is accurate to within ≈1% for our molecular system under the influence of a laser field with an intensity on the order of 10^{12} W/cm^2 and our rotational temperature of 5 K. Calculations were performed for electric fields $E_0/\sqrt{2} = E_{x0} = E_{y0}$ of $\sqrt{2}$, 2, 4, and 6×10^7 V/cm, corresponding to intensities of 0.53, 1.06, 4.25, and 9.56×10^{12} W/cm^2.[19]

For comparison, we also calculate the equivalent classical probability density

$$\rho_{\text{CL}}(\Omega) = e^{-\beta H(\Omega)} / \int e^{-\beta H(\Omega)} \, d\Omega \tag{6}$$

anticipating that the rotational energy-level spacings will be sufficiently small that the much easier classical calculation will prove to be accurate enough to provide a useful approximate way of analyzing the effect of the aligning field.

B. Diffraction Signals. As delineated in our previous work,[4] one may write, within the first-order theory of high-energy electron−molecule scattering, the total scattering intensity for a perfectly clamped N-atomic molecule in a well-defined vibrational eigenstate as

$$I_{\text{total}}(s,\alpha,\Omega) = I_{\text{atomic}}(s) + I_{\text{mol}}(s,\alpha,\Omega) \tag{7}$$

$$I_{\text{atomic}}(s) = I_0 \sigma_{Ru}(s) \sum_j |g_j|^2 \tag{8}$$

$$I_{\text{mol}}(s,\alpha,\Omega) = 2 I_0 \sigma_{Ru}(s) \sum_{j<k} \sigma_{jk}(s,\alpha,\Omega) \quad (j,k = 1, ..., N) \tag{9}$$

Here, I_{total} is the total diffraction signal, which depends on the position on the detector, as defined by s and α, and on Ω which defines the molecular orientation. The expressions ignore any inelastic scattering, because it is featureless, and because its contributions at the large scattering angles of interest to the present work are quite small.[20] I_0 is the incident electron beam intensity, and σ_{Ru} is the Rutherford scattering cross section

$$\sigma_{Ru}(s) = \left(\frac{2 m_e e}{\hbar^2 s^2}\right)^2 \tag{10}$$

with m_e the electron mass and e its charge. The j and k indices label the atoms and the g_j are the complex atomic electron scattering factors, which can be written in terms of an amplitude and a phase[21]

$$g_j(s) = |g_j(s)| \cdot e^{i\eta_j} \tag{11}$$

Simulations of electron diffraction signals conventionally use phenomenological Gaussian broadening functions to account for molecular vibrations.[1] In our work, we account for vibrational motions explicitly by including their exact quantum mechanical probability distribution functions for specific vibrational eigenstates. Structural parameters as well as normal mode vibrational frequencies have been published for tetrazine in the S_0 electronic state.[22,23] However, the full set of normal mode coordinates are not readily available.[24] A consistent set of data was therefore obtained from an ab initio calculation of *s*-tetrazine in the S_0 electronic state. This calculation used the coupled-cluster singles and doubles (CCSD) and the equation of motion coupled-cluster singles and doubles (EOM-CCSD) methods of the ACES II program system.[25] Details of this work will be published elsewhere.[26]

The vibrational temperature of *s*-tetrazine in the cold environment of a free jet expansion is very low, so that to a good approximation all molecules are in their respective ground vibrational states. As has been previously shown, the scattering contributions from individual pairs of atoms can then be expressed as

$$\sigma_{jk}(s,\alpha,\Omega) = |g_j||g_k| \cos(\mathbf{S}\cdot\mathbf{R}_{jk} + \eta_k - \eta_j) \prod_\gamma \langle\psi_\gamma(q_\gamma)| \cos(\mathbf{S}\cdot\mathbf{c}_{jk,\gamma} q_\gamma) |\psi_\gamma(q_\gamma)\rangle \tag{12}$$

Here, $\mathbf{R}_{jk}$ is the vector denoting the equilibrium displacement between the atoms in the molecular frame and the vectors $\mathbf{c}_{jk,\gamma}$ give the contribution of each (mass-weighted) vibrational mode γ to the displacement from the equilibrium.[4] The $\mathbf{S}$ is the momentum transfer vector in the molecular frame. Given the normal modes of the molecule, eqs 12 and 9 readily allow the calculation of the molecular component of the diffraction pattern.

However, eq 7 represents the diffraction signal of molecules that are clamped at specific Euler angles $\Omega = (\theta,\phi,\chi)$. To obtain the diffraction signal of an ensemble of molecules with an orientational distribution function $\rho(\Omega)$, one needs to integrate over all angles

$$I(s,\alpha) = \int I_{\text{total}}(s,\alpha,\Omega) \rho(\Omega) \, d\Omega \tag{13}$$

For an isotropic sample, $\rho(\Omega) = 1/(8\pi^2)$. For samples aligned by the high-intensity lasers we use the results obtained through the use of eqs 5 or 6.

III. Results and Discussion

For all subsequent intensity plots, we keep k_0 fixed at 100 Å^{-1}, corresponding to an incident electron energy on the order of 40 keV, under our assumed high-electron-energy condition, $|\mathbf{k}| \approx |\mathbf{k}_0| \equiv k_0$.

The benchmark for our discussion is the diffraction signal of molecules that are held at perfectly fixed orientations. In the top panel of Figure 2, we show the pattern that results if *s*-tetrazine molecules were clamped such that the plane of the molecule is perpendicular to the incoming electron beam, with the hydrogen atoms aligned along the x axis. The bottom panel of Figure 2 shows the pattern resulting from the molecules clamped in the y,z plane, i.e., with the plane of the molecules aligned with the incoming electron beam. In either case, we plot a modified molecular scattering signal defined as $s_{\text{proj}} \cdot I_{\text{mol}}/I_{\text{atomic}}$, with s_{proj}, I_{mol}, and I_{atomic} as defined in the previous section. The signal intensity is encoded in the color, as shown by the colorbar. The projection of the scattering vector onto the plane of the detector s_{proj} is plotted as the ordinate, whereas the angle α of a detector point, as measured from the projection of the x axis onto the detector, is plotted on the abscissa. Only

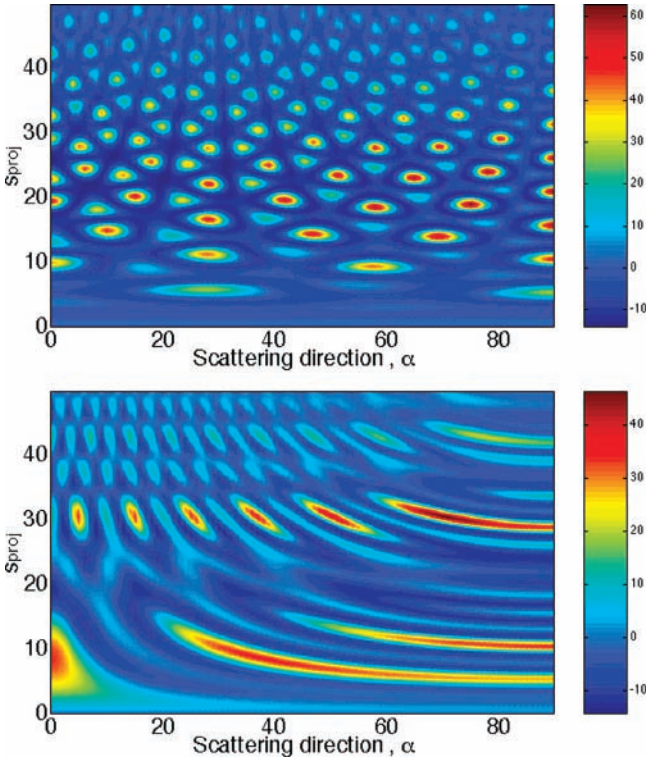

Figure 2. Diffraction patterns of clamped s-tetrazine molecules, $s_{proj} \cdot I_{mol}/I_{atomic}$, plotted as a function of the magnitude of the $x-y$ projected scattering vector s_{proj} and the diffraction direction α. The molecules are assumed to be in their ground vibrational state and the molecular principal axis is fixed to be either parallel with the electron beam (top panel: $\theta = 0°$, $\phi = 0°$, $\chi = 0°$) or perpendicular to the electron beam (bottom panel: $\theta = 90°$, $\phi = 0°$, $\chi = 0°$).

the first quadrant of the diffraction patterns are shown; the others look the same by virtue of the symmetry.

Several points about this figure are striking. First, we note how richly structured the patterns are. In comparison, the patterns of isotropic gas phase molecules would feature horizontal bands only. Clearly, there is a significant amount of information that is lost because of the rotational averaging in conventional gas phase electron diffraction experiments. Second, we note that the patterns are almost fully modulated, at least at small scattering angles. For example, the total intensity ($I_{mol} + I_{atomic}$) of the pattern shown in the top panel of Figure 2 reaches as low as $0.08I_{atomic}$ at $s = 7.4$ Å^{-1} and $\alpha = 30°$. As the magnitude of the scattering vector increases, the modulation depth decreases, presumably because of the damping arising from zero-point vibrational motions. Finally, there is a striking difference in the appearance of the patterns shown in the two panels of Figure 2. In the geometry of the top panel, the molecule is clamped with its plane perpendicular to the electron beam. The electrons therefore are diffracted off the almost hexagonal molecular structure. This hexagonal symmetry is clearly borne out by the diffraction pattern. The diffraction maximum at the smallest diffraction angle shows clear maxima at 60° intervals, corresponding to interferences of wavelets scattered from diametrically opposed ring atoms. In contrast, there is no symmetry in the pattern of the molecules clamped in the y,z plane (bottom panel). The diffraction signal at $\alpha = 0°$ relates to the diffraction of the molecule into a direction perpendicular to its ring. The signal at $\alpha = 90°$ shows the diffraction within the plane of the ring. Clearly, the latter is very sensitive to the internuclear distances, and it shows a large number of tightly spaced modulations.

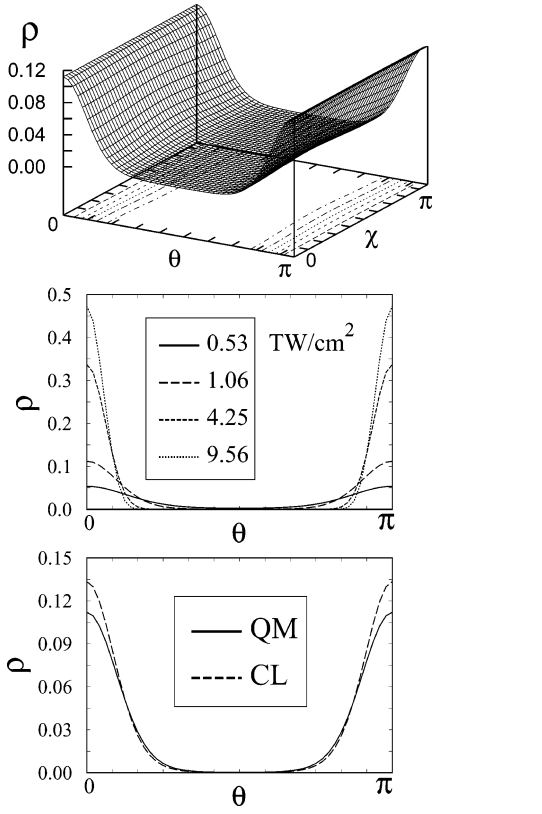

Figure 3. Top panel shows the quantum mechanical orientation distribution ρ (Ω) induced by a circularly polarized laser field acting on a low-temperature *s*-tetrazine molecule (intensity = 1.06×10^{12} W/cm^2, $T = 5$ K). The distribution is independent of ϕ and same distribution repeats itself for the χ range 180°−360°. The middle panel exhibits a cross section of this distribution for $\chi = 0°$ as it varies with the laser power. The bottom panel compares the classical mechanical (CL, dashed) version of the distribution with the quantum mechanically (QM, solid line) generated distribution at an alignment intensity of 1.06×10^{12} W/cm^2.

Alignment of molecules by high-intensity laser fields offers an opportunity to approach clamped molecules in gas-phase samples. Experimentally, laser intensities far in excess of 10 TW/cm^2 can be achieved. However, at the very high intensities, there is a rapidly increasing probability of ionizing the molecule by field ionization.[27] If one assumes an ionization potential of 9.2 eV, as given by the work of Fridh et al.[28] and Gleiter et al.,[29] the approach by Hankin et al.,[30,27] which predicts ion signals based on the Ammosov−Delone−Krainov (tunneling ionization) rate model, would predict a field ionization threshold for s-tetrazine on order of 4×10^{13} W/cm^2. Although the Ammosov−Delone−Krainov model was developed for ionization of atoms, rather than molecules, this threshold agrees well with the experimental onset of ionization observed by Hankin et al.[27]

Figure 3 illustrates the distributions that are obtained with different alignment laser intensities up to 9.56 TW/cm^2. Distributions were calculated for the cases that the alignment laser is incident from the negative x axis and from the negative z axis. Shown in Figure 3 are the results for the latter geometry. Because we assume that the alignment laser is circularly polarized, this distribution is independent of the azimuthal angle ϕ.

As illustrated in the top panel of Figure 3, even with an alignment laser intensity of 1.06 TW/cm^2, the distribution has pronounced maxima at $\theta = 0°$ and 180°, although there is only a very small dependence on the angle χ. These features imply

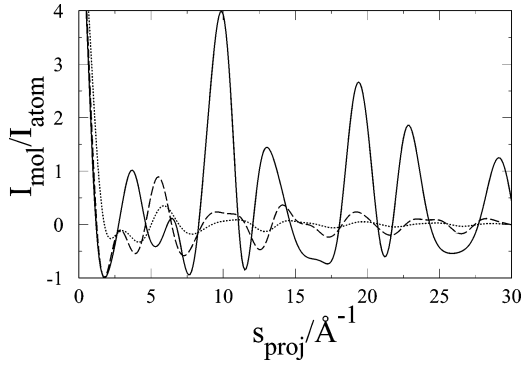

Figure 4. Ratio of molecular to atomic scattering obtained for *s*-tetrazine molecules with the three Euler angles clamped at ($\theta = \phi = \chi = 0°$), solid line; molecules that are clamped only along θ and ϕ, ($\theta = \phi = 0°$), dashed line; and completely isotropic molecules, dotted line. For the completely clamped molecules, the signal along $\alpha = 0°$ is plotted.

that the molecules are preferentially aligned such that their planes coincide with the electric field of the laser, but the molecules are freely rotating about the axis perpendicular to the molecular plane.

The middle panel shows the dependence of the molecular alignment on the alignment laser intensity. Clearly, higher intensities provide for a more pronounced peak of the alignment distribution. The last panel illustrates how quantum effects are reflected in the orientational distribution of the top panel. We note that the classical result captures most of the essential behavior, although the quantum mechanical anisotropy is slightly less spiked than that expected from the classical mechanics calculation. This is a result of typical quantum uncertainty effects. As one might expect, this quantum dispersion is more serious at high alignment intensities, where one approaches the regime in which orientational localization runs into serious uncertainty-principle restrictions. For the case shown in the bottom panel, with an alignment intensity of 1.06×10^{12} W/cm^2, we find $\rho_{CL}/\rho \approx 1.2$ at $(\theta, \chi) = (0°, 0°)$. The ratio increases to 2.8 for the extreme case with 9.56×10^{12} W/cm^2. For all other figures of this paper, we used the fully quantum mechanical distribution functions.

Because the alignment laser acts only on the angles θ and ϕ, while hardly affecting the angle χ, we expect that even under the best circumstances the diffraction patterns will reflect an average over the latter angle. Figure 4 illustrates the ratio of molecular to atomic scattering obtained for completely clamped molecules, molecules that are clamped only along (θ, ϕ), and completely isotropic molecules. The completely clamped molecules show a diffraction pattern that is well modulated up to large diffraction angles. When the curve reaches -1, the molecular scattering is about equal in magnitude but of opposite sign than the atomic scattering, implying that the intensity at that point approaches zero. Note that the clamped-molecule curve shown in Figure 4 is for $\alpha = 0°$; many other traces with different modulation patterns could be drawn for other detector angles, as is evident from Figure 2.

The pattern of the partially clamped molecule is modulated just as much as that of the completely clamped molecule for small diffraction angles. However, at larger scattering angles, the molecular component in the partially aligned case dampens out much more quickly than that of the fully clamped molecule pattern. This suggests that the fact that partial clamping leaves one Euler angle open is not much of a concern at small scattering angles but detrimental at larger angles. If the large angle scattering is an important part of the experiment, an alignment

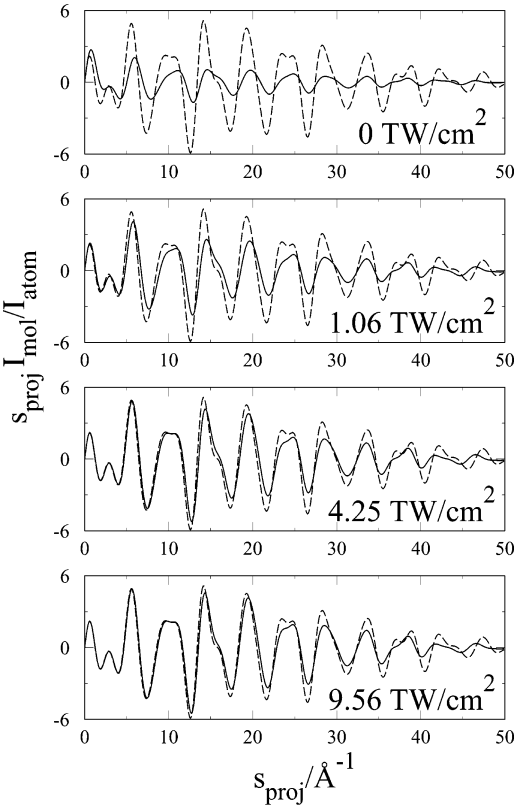

Figure 5. Molecular diffraction signals from isotropic, partially clamped, and *parallel* laser-aligned molecules plotted as the quantity $s_{proj} \cdot I_{mol}/I_{atomic}$. Shown as dashed lines in each panel are the results for the molecules partially clamped at ($\theta = \phi = 0°$), with χ isotropic. The solid lines are, from top to bottom: fully isotropic molecules, molecules aligned with 1.06×10^{12} W/cm^2, molecules aligned with 4.25×10^{12} W/cm^2, molecules aligned with 9.56×10^{12} W/cm^2.

scheme that allows for control of all angles would be preferable. Finally, the pattern of the freely rotating molecules shows the least modulation depth, which is of course observed in conventional electron diffraction experiments. From Figure 4, we conclude that, even though the circularly polarized alignment laser is not able to orient the molecule about all Euler angles, there is a significant benefit stemming from a partial clamping. The modulation depth of the partially clamped molecules is about halfway between that of the freely rotating molecules and that of fully clamped molecules.

With those results in mind, Figure 5 illustrates the molecular diffraction signals of isotropic and laser-aligned molecules in the case the laser is parallel to the electron beam. In all panels, the signal of the (θ, ϕ)-clamped, χ-averaged molecules is shown for comparison as dashed lines. Although the diffraction signal of the freely rotating molecule is very different from the partially clamped molecule, it can be seen that the patterns of the aligned molecules approach that of the partially clamped molecule for high alignment intensities. In fact, it appears that the beneficial effects derived from the alignment laser saturate at about 4 TW/cm^2: the differences between the 4 TW/cm^2 and the 9 TW/cm^2 patterns are very small.

To characterize the similarity between diffraction patterns, we define as a figure of merit the RMS deviation of the difference between two patterns, divided by their average

$$R = \sqrt{\left\langle \left(\frac{(I_1 - I_0)}{\frac{1}{2}(I_1 + I_0)} \right)^2 \right\rangle} \qquad (14)$$

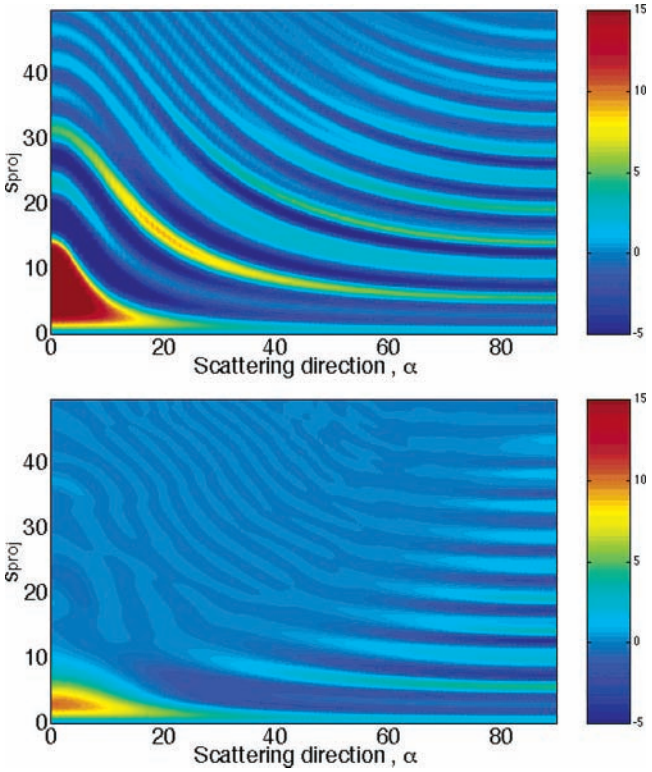

Figure 6. Diffraction from partially clamped and *perpendicularly* laser-aligned s-tetrazine molecules (plotted as $s_{proj} \cdot I_{mol}/I_{atomic}$). Top panel, clamped at ($\theta = 90°$, $\phi = 0°$), with χ isotropic; Bottom panel, aligned in the *y*,*z* plane by a circularly polarized laser pulse with 9.56×10^{12} W/cm^2.

Here, I_1 and I_0 refer to the total signal intensities, i.e., $I_{mol} + I_{atomic}$. The average is taken over diffraction angles up to 50 Å^{-1}. Using this quantity to compare the patterns of Figure 5, we find values of $R = 0.26$, 0.15, 0.06, and 0.05, respectively. We again note that the aligned pattern becomes quite similar to the clamped pattern but that the effect appears to level off above 4×10^{12} W/cm^2.

The consideration of the diffraction patterns for molecules aligned in the *y*,*z* plane by an alignment laser perpendicular to the electron beam becomes more complex because the patterns are no longer cylindrically symmetric. Figure 6 displays a comparison of the (θ, ϕ)-clamped, but χ-averaged, diffraction pattern with the pattern obtained with the 9.56 TW/cm^2 alignment laser impinging from the negative *x* axis. The contour plots show that, although the pattern from the laser-aligned molecules is clearly not as structured as that of the partially clamped molecule, there is a significant similarity in the patterns. In particular at α values approaching 90°, the main features of the modulations are clearly borne out. On the other hand, at small α's, the agreement seems to be less than desirable. This can be understood by recalling that the molecules aligned in the *y*,*z* plane perform a pendular motion in the *x* direction, whereas the partially clamped molecule is strictly confined to that plane. The diffraction signal in the *x* direction (small α) is, understandably, very sensitive toward any displacement of the molecule along the *x* axis.

To quantify these observations we calculated the *R* values, as defined in eq 14, for the patterns of *y*,*z* aligned molecules with alignment intensities from 0 to 9 TW/cm^2, for scattering directions α from 0° to 90°. Figure 7 shows that there indeed is a pronounced minimum at $\alpha = 90°$. At this minimum, the α values are similar to those found with the alignment of the molecular plane perpendicular to the electron beam. The

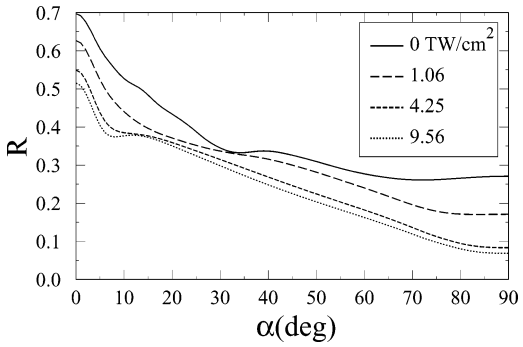

Figure 7. Alignment factor *R*, as defined in eq 14, as a function of α, for *s*-tetrazine aligned in the *y*,*z* plane by a circularly polarized laser pulse with alignment laser intensities as indicated. The *R* values are calculated relative to the partially clamped molecule, with ($\theta = 90°$, $\phi = 0°$) and χ isotropic.

maximum *R* values, however, at $\alpha = 0°$, are significantly larger. This suggests that alignment with high-intensity lasers is very capable of generating patterns quite like those of clamped molecules, unless one observes scattering perpendicular to the ring.

IV. Concluding Remarks

Alignment of molecules by high intensity laser fields is shown to provide a method to increase the modulation contrast and information content of gas phase diffraction patterns. In this study, we restrict ourselves to the case of a circularly polarized alignment laser, acting on a molecule that is almost hexagonal. As a result, the alignment leaves the molecule almost freely rotating about one of the Euler angles. Even so, significant improvement of the diffraction patterns can be achieved for certain orientations. In particular, for diffraction directions that coincide with the distance vector between pairs of atoms, we find a pronounced increase in the modulation depth. In those directions the patterns of aligned molecules quickly approach the ones of clamped molecules, the ideal and limiting case. However, we found that for a scattering direction that is perpendicular to the aligned molecule, the diffraction pattern is a poor match to that of the clamped molecule. We ascribe this to the lack of atom−atom distances in that direction and the residual pendular motion of the molecule.

This study suggests that diffraction experiments of aligned molecules offer an interesting new approach to the determination of molecular structures. The availability of distinct patterns representing diffraction along different planes of the molecule provides additional information content that may help elucidate the structure of larger compounds. As such, the alignment offers a method to extend gas phase diffraction studies to larger molecules, or molecules with lower symmetry, than can presently be done. In addition, alignment may be attractive for selecting specific molecular conformations, for time-resolved studies of chemical reaction dynamics using ultrashort electron pulses and for the mapping of vibrational wave functions in polyatomic molecules. The latter application will be discussed in a forthcoming study.

Acknowledgment. We thank Professor Tamar Seideman and Dr. Bretislav Friedrich for helpful discussions. This work was supported by the Army Research Office under Contract DAAD19-00-1-0141 and by the NSF under Grants CHE-0131114 and CHE-0212823.

Appendix

Evaluation of the matrix elements $\langle J'K'M'|\bar{H}_{ind}|JKM\rangle$ actually reduces to evaluating matrix elements of direction cosines of

the angle that a vector in the molecular frame (here, the transition dipole moment) makes relative to the lab-frame z axis (the incident electron beam direction)

$$\frac{4}{E_{y0}{}^2}\langle J'K'M'|\bar{H}_{\mathrm{ind}}|JKM\rangle =$$
$$\Delta\alpha\,[(1-r)P_{J'K'M'JKM}(2,2,2) + (1-r)P_{J'K'M'JKM}(0,2,2) - P_{J'K'M'JKM}(2,0,2) + rP_{J'K'M'JKM}(0,0,2) - 0.5(1-r)Q_{J'K'M'JKM}] + \Delta\alpha'\,[P_{J'K'M'JKM}(2,0,0) + (1-r)P_{J'K'M'JKM}(2,2,2)] - \Delta\alpha''\,(1-r)P_{J'K'M'JKM}(0,2,0)$$

where

$$r = (E_{x0}/E_{y0})^2$$

$$\Delta\alpha = \alpha_1 - \alpha_2,\ \Delta\alpha' = \alpha_2 - \alpha_3,\ \Delta\alpha'' = \alpha_1 - \alpha_3$$

and

$$P_{J'K'M'JKM}(l,u,w) = \langle J'K'M'|\cos^l\theta\cos^u\phi\cos^w\chi|JKM\rangle$$

$$(l, u, w = 0 \text{ or } 2)$$

$$Q_{J'K'M'JKM} = \langle J'K'M'|\cos\theta\,\sin(2\phi)\,\sin(2\chi)|JKM\rangle$$

Here α_1, α_2, and α_3 ($\alpha_1 > \alpha_2 > \alpha_3$) are the three molecular-frame polarizability components.

We can evaluate the matrix elements P and Q using the explicit expression for the symmetric top basis $|JKM\rangle$[18]

$$|JKM\rangle = \left[\frac{2J+1}{8\pi^2}\right]^{1/2} D^{J*}_{MK}(\phi,\theta,\chi) = \left[\frac{2J+1}{8\pi^2}\right]^{1/2} e^{i\phi M} d^J_{MK}(\theta) e^{i\chi K}$$

where $D^J_{MK}(\phi,\theta,\chi)$ and $d^J_{MK}(\theta)$ are the rotation matrix and the reduced rotation matrix, respectively. Straightforward integrations over ϕ and χ leave us with a single integral

$$R_{J'K'M'JKM}(l) = \int_0^\pi d\theta\,\sin\theta\,\cos^l\theta\,d^{J'}_{M'K'}(\theta)\,d^J_{MK}(\theta), \quad (l = 0, 1, \text{or } 2)$$

with

$$|M' - M| \text{ or } |K' - K| = 0 \text{ or } 2$$

Identifying $d^0_{00}(\theta) = 1$, $d^1_{00}(\theta) = \cos\theta$, and $d^2_{00}(\theta) = 1/2\,(3\cos^2\theta - 1)$, we can express the integral R in terms of the integral S

$$S_{J'K'M'JKM}(l) = \int_0^\pi d\theta\,\sin\theta\,d^{J'}_{M'K'}(\theta)d^l_{00}(\theta)d^J_{MK}(\theta)$$
$$= \sum_{j_1=|J'-l|}^{J'+l}(2j_1+1)\begin{pmatrix} J' & l & j_1 \\ M' & 0 & -M' \end{pmatrix}\begin{pmatrix} J' & l & j_1 \\ K' & 0 & -K' \end{pmatrix} \times \sum_{j_2=|J-j_1|}^{J+j_1}(2j_2+1)\begin{pmatrix} J & j_1 & j_2 \\ M & -M' & M'-M \end{pmatrix}\begin{pmatrix} J & j_1 & j_2 \\ K & -K' & K'-K \end{pmatrix} \times \int_0^\pi d\theta\,\sin\theta\,d^{j_2}_{M'-M,K'-K}(\theta)$$

where $M'-M$ or $K'-K = -2$, 0, or 2, and the Clebsch−Gordon series[31] has been used twice. The last integration can be put in an analytic form, using the explicit expression for $d^j_{mk}(\theta)$[32] with even integers m and k

$$\int_0^\pi d\theta\,\sin\theta\,d^j_{mk}(\theta) = \sum_{\mu=0}^{n} c(\mu;n,a,b)\int_0^\pi d\theta\,\sin\theta\left(\sin\frac{\theta}{2}\right)^{a/2+\mu}\left(\cos\frac{\theta}{2}\right)^{n+b/2-\mu}$$
$$= 2\sum_{\mu=0}^{n} c(\mu;n,a,b)B\left(\frac{a}{2}+\mu+1,\, n+\frac{b}{2}-\mu+1\right)$$
$$c(\mu;n,a,b) = (-1)^\mu\frac{\sqrt{n!(n+a)!(n+b)!(n+a+b)!}}{\mu!(n-\mu)!(a+\mu)!(n+b-\mu)!}$$

where $a = |k-m|$, $b = |k+m|$, $n = j - \max(|m|,|k|)$, and $B(x,y)$ is the beta function.[33]

References and Notes

(1) Hargittai, I. In *Stereochemical Application of Gas-phase Electron diffraction*; Hargittai, I., Hargittai, M., Eds; VCH: Weinheim, Germany, 1988; pp 1−54.

(2) Mott, N. F.; Massey, H. S. W. *The Theory of Atomic Collisions*, 2nd ed.; Oxford: London, 1949; pp 47−49.

(3) Geiger, G. D.; Weber, P. M. *J. Chem. Phys.* **1998**, *108*, 8004.

(4) Ryu, S.; Weber, P. M.; Stratt, R. M. *J. Chem. Phys.* **2000**, *112*, 1260.

(5) Drenth, J. *Principles of Protein X-ray Crystallography*; Springer-Verlag: New York, 1994.

(6) Levine, R. D.; Berstein, R. B. *Molecular Reaction Dynamics and Chemical Reactivity*; Oxford: New York, 1987; pp 480−495.

(7) For general alignment review, see: Friedrich, B.; Pullman, D. P.; Herschbach, D. *J. Phys. Chem.* **1991**, *95*, 8188 and the references therein. Specifically related to the electron diffraction, see: Volker, M.; Meiser, Ch.; Lieschke, J.; Drier, R.; Fink, M.; Böwering, N. *Phys. Rev. A* **1996**, *56*, R1960 and the references therein.

(8) Friedrich, B.; Herschbach, D. *J. Phys. Chem.* **1995**, *99*, 15686.

(9) Seideman, T. *J. Chem. Phys.* **1995**, *103*, 7887. Seideman, T. *Chem. Phys. Lett.* **1996**, *253*, 279. Seideman, T. *J. Chem. Phys.* **1999**, *111*, 4397.

(10) Zon, B. A.; Katsnel'son, B. G. *Sov. Phys.-JETP* **1973**, *38*, 470.

(11) Dudek, R. C.; Weber, P. M. *J. Phys. Chem. A* **2001**, *105*, 4167.

(12) Hoshina, K.; Yamanouchi, K.; Ohshima, T.; Ose, Y.; Todokoro, H. *Chem. Phys. Lett.* **2002**, *353*, 27. Hoshina, K.; Yamanouchi, K.; Ohshima, T.; Ose, Y.; Todokoro, H. *Chem. Phys. Lett.* **2002**, *353*, 33.

(13) Kim, W.; Felker, P. M. *J. Chem. Phys.* **1996**, *104*, 1147. Larsen, J. J.; Mørbak, N. J.; Olesen, J.; Bjerre, N.; Machholm, M.; Rud Keiding, S.; Stapelfeldt, H. *J. Chem. Phys.* **1998**, *109*, 8857. Sakai, H.; Safvan, C. P.; Larsen, J. J.; Hilligsøe, K. M.; Hald, K.; Stapelfeldt, H. *J. Chem. Phys.* **1999**, *110*, 10235. Sugita, A.; Mashino, M.; Kawasaki, M.; Matsumi, Y.; Gordon, R. J.; Bersohn, R. *J. Chem. Phys.* **2000**, *112*, 2164.

(14) Schütz, M.; Hutter, J.; Lüthi, H. P. *J. Chem. Phys.* **1995**, *103*, 7048.

(15) Ab initio theoretical calculations for polarizability anisotropy, especially for the S_0 state, have showed a considerable discrepancy from the experimental values (Heitz, S.; Weidauer, D.; Hese, A. *J. Chem. Phys.* **1991**, *95*, 7952.), suggesting a reexamination of the experimental values. However, theory is in agreement with the experiments on the point that the polarizability anisotropy for the S_1 state is greater than for the S_0 state. For other theoretical values, see ref 24: Josson, D.; Norman, P.; Ågren, H. *Chem. Phys.* **1997**, *224*, 201 and Calaminici, P.; Jug, K.; Köster, A. M.; Ingamells, V. E.; Papadopoulos, M. G. *J. Chem. Phys.* **2000**, *112*, 6301. The three values 60.0, 55.1, and 32.6 au correspond to the molecular-frame polarizability components, α_1, α_2, and α_3, respectively, of the Appendix.

(16) Larsen, J. J.; Hald, K.; Bjerre, N.; Stapelfeldt, H.; Seideman, T. *Phys. Rev. Lett.* **2000**, *85*, 2470.

(17) Pershan, P. S.; van der Ziel, J. P.; Malstrom, L. D. *Phys. Rev.* **1966**, *143*, 574. Stapelfeldt, H.; Seideman, T. *Rev. Mod. Phys.* **2003**, *75*, 543.

(18) Zare, R. N. *Angular Momentum*; John Wiley & Sons: New York, 1988; p 105.

(19) Besides orienting our molecule, the strong electric fields being employed here could, in principle, affect the dynamics of the diffracting electrons themselves. However, our estimates suggest that there will be no significant direct effects on the 40 keV electron trajectories. Consistent with the independent-atom approximation for the electron scattering, we also do not anticipate any significant indirect perturbations caused by field-induced molecular dipoles.

(20) Bonham, R. A.; Fink, M. *High Energy Electron Diffraction*; ACS Monograph, van Nostrand Reinhold: New York, 1974.

(21) *International Tables for Crystallography*; Wilson, A. J. C., Ed.; Kluwer Academic: Dordrecht, 1991; Vol. C.

(22) Innes, K. K.; Franks, L. A.; Merer, A. J.; Vermulapalli, G. K.; Cassen, T.; Lowery, J. *J. Mol. Spec.* **1977**, *66*, 465.

(23) Brumbaugh, D. V.; Haynam, C. A.; Levy, D. H. *J. Mol. Spec.* **1982**, *94*, 316.

(24) Selected theoretical normal mode coordinates have been published in Stanton J. F.; Gauss, J. *J. Chem. Phys.* **1996**, *104*, 9859.

(25) Advanced Concepts in Electronic Structure Theory (ACES II) is a program product of the Quantum Theory Project, University of Florida. Authors: Stanton, J. F.; Gauss, J.; Watts, J. D.; Nooijen, M.; Oliphant, N.; Perera, S. A.; Szalay, P. A.; Lauderdale, W. J.; Gwaltney, S. R.; Beck, S.; Balková, A.; Bernholdt, D. E.; Baeck, K. K.; Rozyczko, P.; Sekino, H.; Hober, C.; Bartlett, R. J. Integral packages included are VMOL (Almöf, J.; Taylor, P. R.); VPROPS (Taylor, P. R.); ABACUS (Helgaker, T.; Jensen, H. J. Aa.; Jorgensen, P.; Olsen, J.; Taylor, P. R.).

(26) Ryu, S.; Stratt, R. M.; Baeck, K. K.; Weber, P. M. (to be published).

(27) Hankin, S. M.; Villeneuve, D. M.; Corkum, P. B.; Rayner, D. M. *Phys. Rev. A* **2001**, *64*, 013405.

(28) Fridh, C.; Åsbrink, L.; Jonsson, B. Ö.; Lindholm, E. *Int. J. Mass. Spectrom. Ion Phys.* **1972**, *9*, 485.

(29) Gleiter, R.; Heilbronner, E.; Hornung, V. *Helv. Chim. Acta* **1972**, *55*, 255.

(30) Hankin, S. M.; Villeneuve, D. M.; Corkum, P. B.; Rayner, D. M. *Phys. Rev. Lett*. **2000**, *84*, 5082.

(31) Reference 18, p 99.

(32) Reference 18, p 88.

(33) *Handbook of Mathematical Functions*; Abramowitz, M., Stegun, I. A., Eds.; Dover: New York, 1965; p 258.